2020 NDIA GROUND VEHICLE SYSTEMS ENGINEERING AND TECHNOLOGY SYMPOSIUM
MOBILITY TECHNICAL SESSION
AUGUST 11-13, 2020 - NOVI, MICHIGAN

Degradation/ Mitigation of Li-ion Batteries for High Rate Discharge Applications

Tony Thampan, PhD, Yi Ding, PhD, Laurence Toomey, PhD

U.S. Army Combat Capabilities Development Command (CCDC)

Ground Vehicle Systems Center

ABSTRACT

The U.S. Army has been pursuing vehicle electrification to achieve increased combat effectiveness and new capabilities, potentially requiring high power pulse duty cycles. However as Energy Storage System (ESS) pulse power discharge rates (> 40 C rate) increase, there is a significantly lower ESS lifetimes. Results of high power pulse duty cycles on lithium iron phosphate cell lifetime performance show a dramatic loss. For 2s and 3s, 120 A pulse tests, the observed degradation after 80 hours cycling is 22 % and 32 % respectively, significantly higher than previously reported values at lower discharge rates, but similar temperatures. A 7 year calendar aged cell was also tested with a 2s pulse and showed severe degradation (53% loss after 40 hours cycling). The decreased lifetime of the high pulse duty cycling aged cells is a result of the increased strain / heating at high currents, and subsequent SEI fracture, and thermally accelerated SEI formation. This mechanism leads to lithium consumption at the anode, and eventual capacity loss. To mitigate the pulsing induced thermal degradation, the use of different thermal management systems based on immersion cooling is proposed based on simulation results.

Citation: T. Thampan, Y. Ding, L.Toomey, A. Hundich, V. Babu, "*Accelerated degradation of Li-ion Batteries for High Rate Discharge Applications*", In *Proceedings of the Ground Vehicle Systems Engineering and Technology Symposium* (GVSETS), NDIA, Novi, MI, Aug. 11-13, 2020.

1. INTRODUCTION

The U.S. Army has been pursuing vehicle electrification to achieve enhanced combat effectiveness. The benefits of vehicle electrification via hybridization with Energy Storage Systems (ESS) include significant fuel savings / range extension, increased silent watch / mobility and new capabilities in Electronic Warfare (EW), High Power Sensors and Directed Energy (DE) systems[1].

The discharge rates* for silent mobility, a 30 kW DE and 100 kW DE capability using a Hybrid Electric Vehicle (HEV) configuration are shown in Figure 1, along with examples of commercial systems.

The silent mobility power requirements has been normalized for combat vehicle platform weight (3.9kW/t) and the battery pack is proportionally sized (0.6 kWh/t). Thus the discharge rate for the silent mobility capability is constant across different platform sizes. This discharge rate can be met using existing HEV ESS solutions[2]. However, as the platform size decreases, the ESS discharge rates for DE capabilities increases significantly beyond standard HEV ESS solutions. In these pulse power applications, the high power pulse duty-cycles[3] can have discharge rates that are significantly higher (> 10C) than commercial HEV ESS systems, resulting in increased thermal and electrical stress.

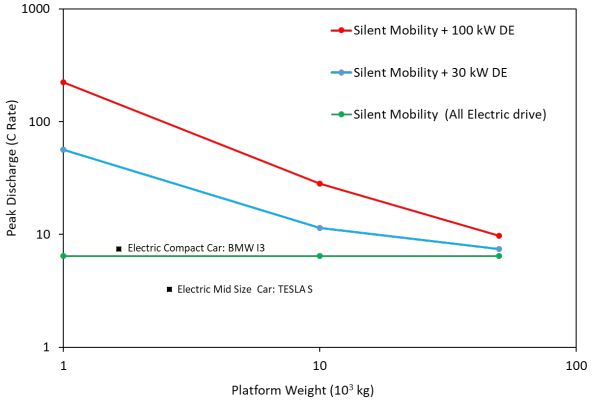

Figure 1: Battery capacity normalized with platform size to provide silent mobility and directed energy capabilities

2. Previous Work

There has been limited published experimental work on high rate discharge. Wong et al. tested $LiNi_xCo_yAl_{1-x-y}O_2$, (NCA)[4] and $LiFePO_4$ (LFP)[5] for pulsed at high rate. For the LFP cells tested at 15C discharge rate, the rapid cell capacity decay was attributed to the increase in cell resistance and not the loss of active material.

Cell degradation theory and prediction is critically important to multiple commercial applications and is an active area of research. Models have been proposed based on empirical[6] and physics based aging mechanisms[7,8].

Based on previous work, the cell degrades due to the consumption of active Li material via solid electrolyte interphase (SEI) growth[9] as shown in Figure 2.

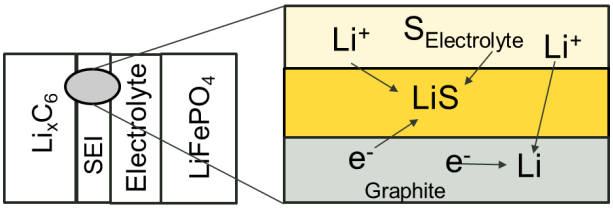

Figure 2 The desired electrochemical reaction is the lithium intercalation in graphite, but lithium can also react with components of the electrolyte to form a solid-electrolyte interphase.

3. Experimental

Based on the use of LFP cells in commercial pulse power applications such as power tools and long life time, a 26650 LFP cell was selected. The cell properties are shown in Table 1.

Table 1 26650 LFP Cell

Description	Value
Nominal Capacity	2.3 Ah
Nominal Voltage	3.3 V
Maximum Pulse Discharge	120A
Cycle life at 10C/ 100% DOD	1000 cycles
Cut Off Voltage	2.0 V
Cell weight	70g

The cells were attached to an A&D / BITRODE electronic load with thermocouples affixed to the cell skin surface. The cells were then placed into a thermal chamber for environmental control at 10°C for automated lifetime cycling testing. The test schedule is shown in Table 2.

Table 2 LFP Pulse schedule

* Standard industry practice is to define charging / discharging by C rates. By definition a 1 C rate discharge is equivalent to a discharge current will discharge the entire battery in 1 hour.

Step	Description
1	10A charge to 100% SOC / 3.6 V
2	120 A for *t* seconds, followed by 8 s cooling
3	Step (2) repeats until 0% SOC / 2.0V
4	Temperature and Capacity measured
5	Return to Step (1)

4. Results

Figure 3 shows the cell's voltage and current response to a load profile as shown in Table 2 with a 120 A pulse for 2 s. It can be seen the cell can sustain the pulse for 6 mins before it reaches the 2 V discharge limit. It is then charged for 13 minutes before it reaches 3.6 V / 4 A limit. The initial capacity with this profile was 1.84 Ah. The cell under a 120 A pulse for 3s, shows a similar profile, with an initial capacity of 1.95 Ah.

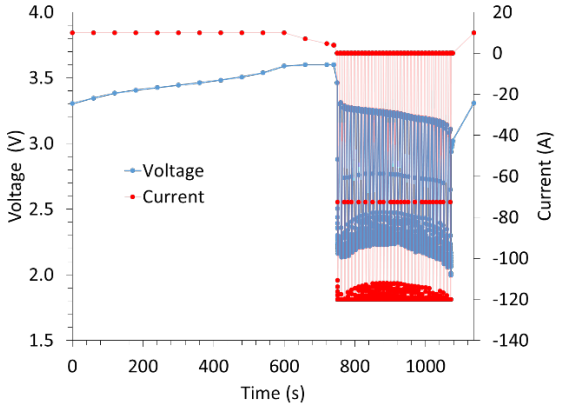

Figure 3 Current and Voltage Characteristics of LFP 2.3 Ah under test during charge and discharge

As shown in Figure 4, the heat generation due to the 3s 120A pulse increases the cell skin temperature to 58°C. This is significantly higher than the 41°C maximum observed during the 2s pulse profile. Both cells cool during the charge profile, due to the 10°C ambient air cooling.

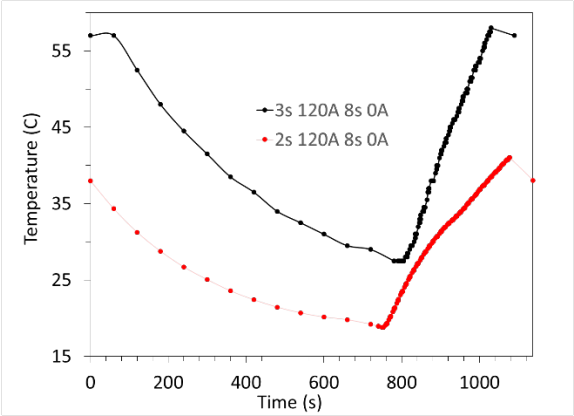

Figure 4 Temperature characteristics of test during charge and discharge. Heating occurs during discharge at 120A pulses. Cooling occurs during charge at 10A. Ambient temperature is 10°C.

The degradation data is shown in Figure 5, where capacity loss is based on initial cycle capacity during the pulse profile. The 3s 120A pulse shows higher degradation (32%) than the 2 s 120 A pulse (22%) after 250 cycles. The degradation is substantial higher for the 3s pulse, which may occur due to higher temperature.

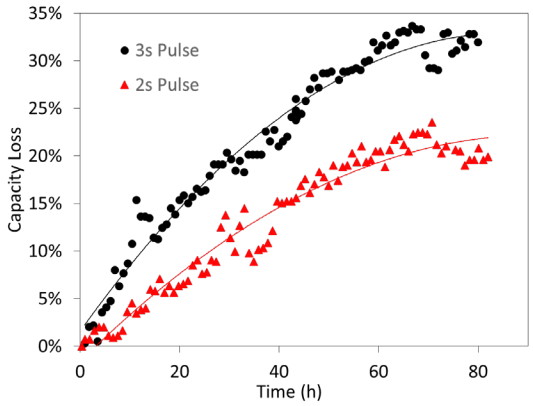

Figure 5 LFP 2.3 Ah cell capacity loss with 120 A / 55 C pulsing for 2s and 3s. The degradation time observed (5000 mins) corresponds to 250 cycles and is significantly lower than 1000 cycle design target

Figure 6 shows the effect of long term storage (7 year) with a 2s 120A high pulse duty cycling. The capacity after storage was measured at 1.74 Ah. The 7 year calendar aged cell showed severe degradation with the 2s high duty cycle pulse vs the cell that was tested with the 2s high duty cycle

pulse with no calendar aging, a 53% loss vs 15% after 40 hrs cycling, respectively.

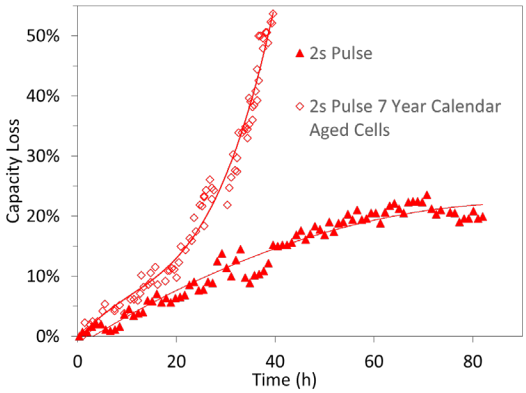

Figure 6 LFP 2.3 Ah cell capacity loss with 120 A / 55 C pulsing for 2s without calendar aging and with 7 year calendar aging. The degradation observed with the calendar aged cell shows substantial acceleration vs the cycle aged cell only.

5. Discussion

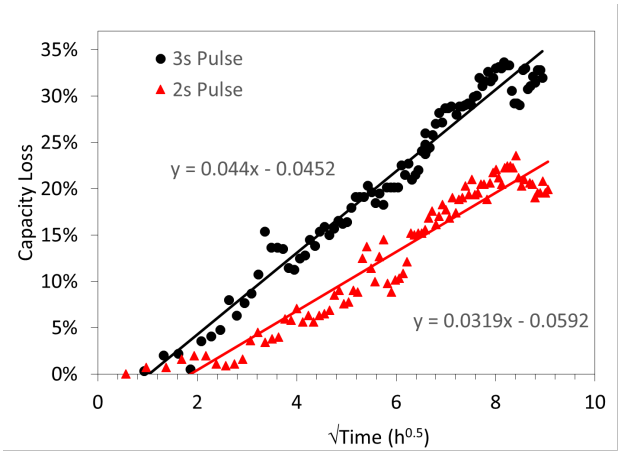

Figure 7 2.3 Ah cell capacity loss vs $t^{0.5}$. The degradation trend line suggests the dominant degradation is SEI growth consuming active material (Li)

Based on previous work[10,11] the dominant degradation mechanism is SEI growth by consumption of active material, *i.e.* Li.

Assuming that capacity loss (Q_{loss}) is based on the SEI consumption of lithium (J_{SEI}):

$$Q_{loss} = \int_{t_0}^{t} J_{SEI}\, dt \qquad \text{Eq.1}$$

And assuming that the SEI thickness (s) growth is first order:

$$\frac{ds}{dt} = \frac{J_{SEI} m_{massSEI}}{\rho A_{SEI}} = \frac{k\, D_{Li}\, C^0}{1 + k\, s} \qquad \text{Eq. 2}$$

Where is C^0 the bulk electrolyte concentration, D_{Li} is the diffusion coefficient and k is the rate constant. It can be shown for large time[11]:

$$Q_{loss} = K_1\sqrt{D_{Li} t} - \frac{D_{Li}}{k} \qquad \text{Eq.3}$$

with K_1 as a constant. Thus if SEI growth is dominating capacity loss, a plot of capacity loss vs. $\sqrt{t}$ should be linear. This is shown in Figure 7, suggesting SEI growth causes the observed degradation. Furthermore based on Eq. 3, the magnitude of the temperature increased capacity rate (0.044 vs. 0.0319), should be similar to the increase in the temperature dependent variables in Eq. 3, which is D_{Li}. Utilizing a reported activation energy value of D_{Li}. (0.52 eV)[11], it can be shown that the increased temperature degradation rate is similar to the increased D_{Li} at higher temperatures ($4.8\ 10^{-17}$ vs $2.62\ 10^{-17}$ cm^2/s). This increases confidence that capacity loss results from SEI growth consuming Li.

The calendar year storage with the high pulses appears to have increased the degradation rate. Based on the degradation rate observed (Fig 6), it does not appear that Li consumption and loss, is mitigated with time by SEI formation. The degradation rate is divided, with 2 different linear zones. The subsequent zone is accelerated compared to the initial zone, suggesting that when the initial SEI has delaminated, a new SEI layer is forming leading to an increase in the degradation rate.

Figure 8 and 9 show degradation rates (best fit) of the high pulse duty cycling (55C Rate) experiments compared to previous reported degradation data at lower rates[6]. The peak temperature for the 2s 120A high pulse duty cycling is 41℃, and for the 3s, the peak temp was 58℃. Thus these data sets were compared to data reported at 45℃ and 60℃, respectively. It can be seen that the high pulse duty cycling degradation rates are significantly higher than the lower discharge rates, though similar in trend. This suggests that the high pulse duty cycling introduces high strain into the graphitic

anode leading to a much higher rate of SEI fracture, formation and Li consumption, before the SEI limits Li diffusion and subsequent capacity degradation.

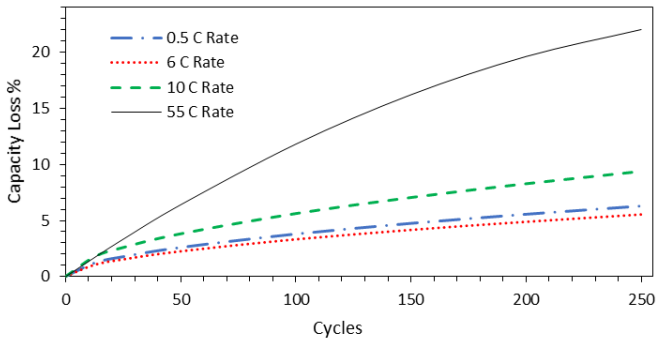

Figure 8 Comparison of capacity loss at different discharge rates with cycle number for 2s pulse at 55 C rate and constant 0.5 C, 6 C and 10 C rates at 45°C

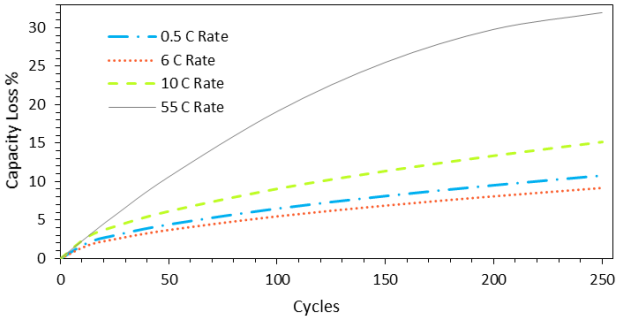

Figure 9 Comparison of capacity loss at different discharge rates with cycle number for 3s pulse at 55 C rate and constant 0.5 C, 6 C and 10 C rates at 60°C.

6. Degradation Mitigation

Considering that SEI growth increases with temperature, improved heat removal should mitigate pulse induced degradation.

To better evaluate the heat removal, a thermal model of the 26650 LFP cell was developed. Utilizing the high pulse discharge data and Hybrid Pulse Power Characterization Test data, a 2 RC equivalent circuit was fit. Utilizing the energy equation, it is possible to estimate the temperature profile in the cell. Utilizing a ANSYS CFD tool and cell data[12] it is possible to estimate the temperature profile on the cell.

Due to the cell construction, the cell's thermal conductivity is lower in the radial direction than the axial direction, resulting in the resulting profile on the cell as shown in Figure 10.

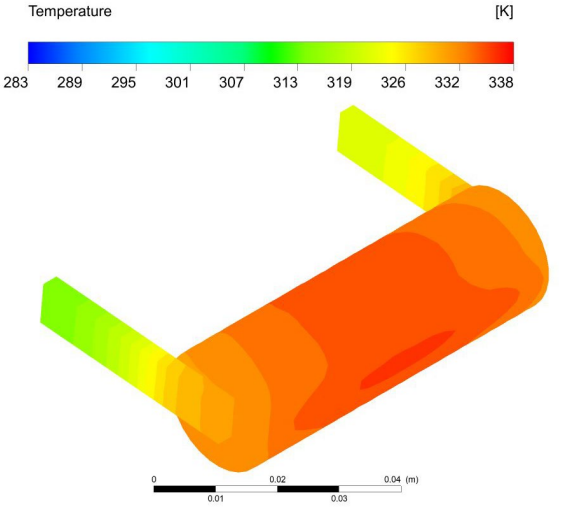

Figure 10. The temperature profile (K) on the cell surface and tabs. The cell is in a convective thermal chamber (283K).

However although cell surface temperature is usually monitored, it is critical to estimate the internal cell temperature.. This is shown in Figure 11. It can be seen that while certain parts are cooler due to the tabs, the hottest part of the cell is towards the center.

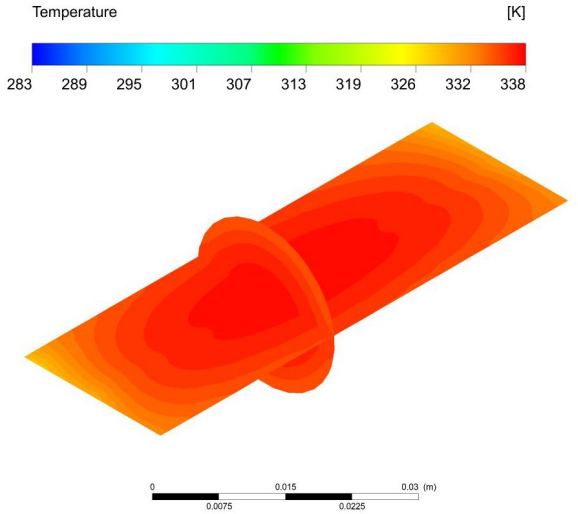

Figure 11 Internal cell temperature (K) in the axial and radial plane. Internal cell temperature is cooler towards tabs and hottest in the center.

Thus it is important to design the cell to ensure enough heat is removed to avoid thermal hot spots

and subsequent degradation. This can be done by alternative cell design and cooling. As shown in Figure 12, the temperature rise mitigated by liquid cooling.

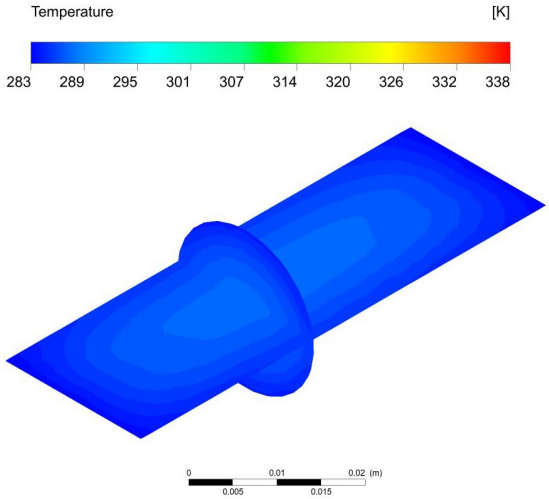

Figure 12 Internal cell temperature (K) in the axial and radial plane when cell is liquid cooled at 283K

A further means to limiting temperature increase is to decrease heat generation due to resistive heating during high pulse duty cycling. This can be done using commercially cells optimized for power. Figure 13 shows a comparison based on commercially available Ultra High Power and Ultra High[13] Energy cells. It can be see that for the same heat removal, the power cells provide more peak power, than the energy cell. This is done by designing the cell resistance to be lower, however the consequence is lower available energy, 1.7 x less energy for 1.5 x more power.

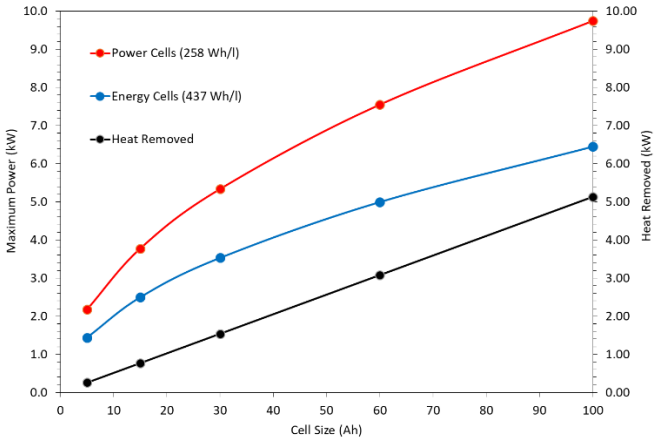

Figure 13 A comparison of cells optimized for power vs energy. For the identical heat removal, Power Cells offer more peak power performance (+1.5X) at the cost of energy (-1.7X), vs. Energy Cells

7. Conclusion

Based on pulsed discharge, accelerated degradation was observed on LFP cells. The degradation increased based on the duration of the pulse, potentially due to the higher temperature observed due to increased joule resistive heating. Based on preliminary analysis, it appears that lithium loss due to SEI growth is dominant loss mechanism. Future work involves model development to predict failure at different conditions and additional cell characterization techniques to further elucidate degradation mechanisms and identify mitigation measures using immersion cooling.

1. REFERENCES

1 Ed Mazzanti, MG R. M. Dyess, ARCIC, US ARMY October, 2017,
2 D. Erb, PhD Thesis, Massachusetts Institute of Technology 2016
3 J. Nairus, et al DOD Energy & Power S&T Roadmap, September, 2017
4 D. Wong, B Shrestha, D Wetz, J Heinzel, J. Power Sources, 363-372 (280), 2015
5 D. Wong, D. Wetz, J. Heinzel, A. Mansour, J. Power Sources 81-90 (328), 2016
6 J. Wang, P. Liu, J. Hicks-Garner, E. Shermana, S. Soukiaziana, M. Verbrugge, H.Tatariab, J. Musser, P. Finamore, J. Power Sources 3942–3948(196), 2011
7 M. Schimpe, M. E. von Kuepach, M. Naumann, H. C. Hesse, K. Smith, and A. Jossen, J. Electrochemical Soc., A181-A193 165 (2) 2018

8 R. Deshpande and D Bernardi, J. Electrochemical Soc., A461-A474 164 (2) 2017
9 E. Peled and S. Menkin, J. Electrochemical Soc., A1703-A1719 164 (7) 2017
10 M. Broussely, S. Herreyre, P. Biensan, P. Kasztejna, K. Nechev and R.J. Staniewicz, J. Power Sources 13-21 (97-98) 2001
11 M. B. Pinson and M. Bazant, J Electrochem. Soc., A243-A250 160 (2), 2013